OSCILLATORY BEHAVIOR OF ASYMPTOTIC-PRESERVING SPLITTING METHODS FOR A LINEAR MODEL OF DIFFUSIVE RELAXATION

JEFFREY R. HAACK AND CORY D. HAUCK

JEFFREY HAACK

Department of Mathematics
University of Wisconsin, 480 Lincoln Drive, Madison, Wisconsin 53706

CORY HAUCK

Computational Physics Group (CCS-2) and Center for Nonlinear Studies (T-CNLS)
Mail Stop B258, Los Alamos National Laboratory, Los Alamos, New Mexico 87544

ABSTRACT. The occurrence of oscillations in a well-known asymptotic preserving (AP) numerical scheme is investigated in the context of a linear model of diffusive relaxation, known as the P_1 equations. The scheme is derived with operator splitting methods that separate the P_1 system into slow and fast dynamics. A careful analysis of the scheme shows that binary oscillations occur due to a staggered diffusion stencil and that dispersive-type oscillations occur because there is too little numerical dissipation. The latter conclusion is based on comparison with a modified form of the P_1 system. Numerical fixes are also introduced to remove the oscillatory behavior.

1. **Introduction.** In this paper, we examine oscillatory behavior in asymptotic-preserving (AP) operator-splitting techniques for the so-called P_1 *equations* in one spatial dimension. These equations form a simple 2×2 linear hyperbolic system which serves as a rough approximation of more complicated kinetic descriptions of particle transport through a material medium [26, 39]. Operator splitting is one approach to computing numerical solutions to such systems and, in the current context, they are particularly useful in multi-scale applications with diffusive relaxation, which we describe below. In practice, the P_1 system serves as a prototype for more complicated moment systems. For our current purposes, we focus on this system in order to make the numerical analysis of the operator splitting more transparent.

In kinetic models of particle transport, diffusive relaxation is a common phenomena that occurs when the mean free path between particle collisions with a material medium is small when compared to the macroscopic scales of interest. In such cases, particles undergo frequent collisions with the material so that, over long time scales, the predominant macroscopic behavior of the system is diffusive [23, 26, 39].

Even though particle transport in collisional regimes can be accurately approximated with a diffusive model, a kinetic model is still needed for regimes in which collisions are less frequent. Thus, when simulating multi-scale problems with regions of both high and low collisionality, such as multiple materials, a reasonable approach is to use a kinetic model everywhere, since it is valid for all regimes. The challenge of such an approach is to develop numerical methods that mimic the asymptotics of the diffusion limit at the discrete level *without resolving temporal and spatial scales associated with the mean free path*, which tends to zero in the diffusion limit. In particular, a numerical scheme for a kinetic model should be consistent with the diffusion equation in the diffusion limit. This is the so-called *asymptotic preserving property* [16].

Conventional Godunov-type solvers for kinetic models, based on spatial reconstructions and upwinding, are typically not asymptotic preserving. Like almost all hyperbolic solvers, these methods use numerical dissipation to maintain stability around discontinuities, and in most cases, the dissipation increases as the system approaches the diffusion limit. Eventually, the numerical dissipation will actually dominate the physical diffusion in the system. Consequently, one may generate results which appear to resolve the solution profile, but are far from accurate.

Several methods have been developed for the P_1 equations and related systems which are AP in the diffusive limit. We mention in passing the well-balanced approach taken in [10, 11, 2] and the discontinuous Galerkin formulation used in [24, 29, 32]. However, our focus here is the AP operator splitting methodology that has been developed over the last ten years, with applications to discrete-velocity kinetic models [20], radiative transfer [21], and kinetic semiconductor equations [18]. A complete review of this methodology can be found in [19]. Unlike naive splitting approaches that are based solely on simplifying the numerical implementation of a model, AP splitting is done in such a way as to preserve asymptotic balances. In the context of diffusive relaxation, this means separating a given kinetic model into two component systems with the following properties:

1. One component contains fast dynamics related to the mean free path. It is numerically stiff and therefore updated in time with an implicit method. Although implicit, the update is much simpler than an implicit update of the full model and can often be implemented in an explicit fashion.
2. The second component contains slower, macroscopic dynamics and can be updated with a standard explicit method.
3. As an isolated system, each component is well-posed in some sense.

The evolution of the complete system is performed by alternately updating each of the two components. Such an approach is first order in time, but can improved with more complex time integrators, such as implicit-explicit IMEX schemes [1, 37, 38].

Although successfully implemented in a number of applications, the operator splitting methodology has some subtle issues. One of these is the onset on spurious oscillations which are stable, but lead to unphysical results. Often, such oscillations arise in so-called *transition regimes*, where collisions play an important role in the dynamics of the model, but are not frequent enough to validate the diffusion limit. Moment equations for simulating transport are most useful in these regimes, either as stand-alone models or as preconditioners for more complex models.

The cause of spurious oscillations in the operator splitting is not easily deduced from inspection of the two component systems individually. Rather, one must look at the composition of the two components as a single method. Previously, it has

been conjectured that oscillations and instabilities might be attributed to numerical dispersion terms [16] or to numerical diffusion terms defined on staggered grids [15], both of which are numerical artifacts of the splitting that appear in the full scheme. We confirm here that binary oscillations can occur in low-resolution schemes as a result of the staggered grid. However, we also determine that oscillations of a dispersive nature can be attributed to a lack numerical dissipation in the scheme, as opposed to standard upwind methods which are often overly dissipative. Our analysis is based on a comparison with a modified version of the P_1 system, which was first introduced in [16] and later generalized in [15].

The organization of the paper is as follows. In Section 2, we introduce the P_1 equations, their properties, and approaches for computing numerical solutions. In particular, we identify the challenges associated with upwind methods and how a splitting approach can be used to attack these challenges. We also exhibit cases where the splitting scheme is oscillatory. In Section 3, we investigate the first order version of the splitting scheme in more detail. This includes diagnosing the source of oscillations and implementing corrections. Results are presented to exhibit improvement effected by our corrections. Section 4 contains discussion and conclusions. Finally, details of numerical schemes are given in the Appendix.

2. **The P_1 System.** The P_1 system, also known as the *hyperbolic heat equation* [4, 3, 13], is a relaxation model formulated as a simple 2×2 system. In one space dimension, and with a diffusive scaling, the nondimensional equations are

$$\partial_t \rho + \partial_x m = 0 \,, \tag{1a}$$

$$\partial_t m + \frac{1}{3} \frac{1}{\varepsilon^2} \partial_x \rho = -\frac{\sigma}{\varepsilon^2} m \,. \tag{1b}$$

These equations are derived from a kinetic transport equation [26, 39, 15], and the variables ρ and m are the first two moments of the underlying kinetic distribution function. Physically, ρ is the concentration of particles and εm is the bulk momentum, where the parameter ε is the magnitude of the macroscopic reference velocity relative to the microscopic particle velocity. Finally, $\sigma = \sigma(x)$ is the non-dimensional scattering cross-section. Given a macroscopic length scale L, the physical cross-section (the inverse of the mean free path) is $\varepsilon L \sigma$.

The mathematical aspects of the P_1 system and its nonlinear variants—including the diffusive asymptotic behavior—have been studied both theoretically [27, 22, 33, 30, 31, 35] and numerically [10, 29, 20]. Studies of related models can be found in the context of radiation and neutron transport [34, 25, 2, 11, 32] and also in drift-diffusion systems such as charge transport in semiconductors [14, 21, 36] and chemotaxis [7, 6].

Upon diagonalization, the P_1 equations take the form of a Goldstein-Taylor model [9, 41] with wave speeds $\pm(\sqrt{3}\varepsilon)^{-1}$. Indeed, if we set $\phi^\pm = \rho \pm \sqrt{3}\varepsilon m$, then

$$\partial_t \phi^+ + \frac{1}{\varepsilon} \frac{1}{\sqrt{3}} \partial_x \phi^+ = -\frac{\sigma}{2\varepsilon^2} (\phi^+ - \phi^-) \,, \tag{2a}$$

$$\partial_t \phi^- - \frac{1}{\varepsilon} \frac{1}{\sqrt{3}} \partial_x \phi^- = -\frac{\sigma}{2\varepsilon^2} (\phi^- - \phi^+) \,. \tag{2b}$$

Meanwhile, the diffusive character of (1) is evident upon formally balancing powers of ε in (1b) to specify a closure for (1a) that is accurate up to $O(\varepsilon^2)$:

$$m = -\frac{1}{3\sigma}\partial_x\rho\,, \tag{3a}$$

$$\partial_t\rho = \partial_x\left(\frac{1}{3\sigma}\partial_x\rho\right)\,. \tag{3b}$$

In the following subsections, we review schemes for the P_1 system based on both upwinding and splitting. Because these schemes are not new, many of the details of their implementation have been moved to the appendix.

2.1. **Upwind Discretization.** Upwind discretizations of (1) and similar equations are known to have difficulties in diffusive regimes [29, 17, 20, 36, 8]. For fixed mesh spacing h, there are two related issues that arise in the limit $\varepsilon \to 0$: (i) excessive numerical dissipation and (ii) a restrictive time step. Both are easily understood by way of a semi-discrete, first-order, upwind scheme for (2):

$$d_t\phi_j^+ + \frac{1}{\varepsilon}\frac{1}{\sqrt{3}}\frac{\phi_j^+ - \phi_{j-1}^+}{h} = -\frac{\sigma_j}{2\varepsilon^2}(\phi_j^+ - \phi_j^-)\,, \tag{4a}$$

$$d_t\phi_j^- - \frac{1}{\varepsilon}\frac{1}{\sqrt{3}}\frac{\phi_{j+1}^- - \phi_j^-}{h} = -\frac{\sigma_j}{2\varepsilon^2}(\phi_j^- - \phi_j^+)\,, \tag{4b}$$

which, in terms of ρ and m, takes the form

$$\partial_t\rho_j + \frac{m_{j+1} - m_{j-1}}{2h} = \frac{h}{2\varepsilon}\frac{1}{\sqrt{3}}\frac{\rho_{j+1} - 2\rho_j + \rho_{j-1}}{h^2}\,, \tag{5a}$$

$$\partial_t m_j + \frac{1}{\varepsilon^2}\frac{1}{3}\frac{\rho_{j+1} - \rho_{j-1}}{2h} + \frac{\sigma}{\varepsilon^2}m_j = \frac{h}{2\varepsilon}\frac{1}{\sqrt{3}}\frac{m_{j+1} - 2m_j + m_{j-1}}{h^2}\,. \tag{5b}$$

Here, and for the remainder of this paper, the subscript j for state variables ρ and m and the crossection σ denotes the average value of the respective quantity over a computational cell I_j of width h. Later, we will also introduce composite parameters γ_j, κ_j, and β_j, which depend on σ_j.

For ε small, the dominant balance in (5b) is

$$m_j = -\frac{1}{3\sigma_j}\frac{\rho_{j+1} - \rho_{j-1}}{2h} + O(\varepsilon)\,, \tag{6}$$

which when substituted into (5a), gives

$$\partial_t\rho_j = \frac{1}{3}\frac{\sigma_{j+1}(\rho_{j+2} - \rho_j) - \sigma_{j-1}(\rho_j - \rho_{j-2})}{4h^2} + \frac{h}{2\varepsilon}\frac{1}{\sqrt{3}}\frac{\rho_{j+1} - 2\rho_j + \rho_{j-1}}{h^2} + O(\varepsilon)\,. \tag{7}$$

As $\varepsilon \to 0$, the first term on the right hand side of (7) yields a consistent discretization of the diffusive flux on the right hand side of (3b). However, the second term on the right hand side of (7)—the numerical dissipation term—will clearly affect the accuracy of the solution unless the mesh spacing h is chosen much smaller than ε—an expensive undertaking given that one need not resolve such small scales when discretizing the diffusion equation (3b) directly. The expense of resolving ε is exacerbated by a stiff hyperbolic CFL condition which requires that the time step Δt in any temporal discretization of (5) satisfies

$$\Delta t < \varepsilon C h \tag{8}$$

for some $O(1)$ constant C.

The dissipative nature of the upwind scheme (5) is exhibited by the numerical solutions of the P_1 equations presented in Figures 1(a) and 1(c), where temporal integration of the semi-discrete scheme is achieved using first-order, semi-implicit method: the fluxes are evaluated explicitly, but the source term in (5b) is handled implicitly. Solutions are computed for $x \in [0,2]$, with a constant cross-section $\sigma = 1.0$, periodic boundary conditions, and initial conditions given by

$$\rho = \left\{ \begin{array}{ll} 2.0 \,, & x \in [0.8, 1.2] \,, \\ 0.0 \,, & x \in [0.0, 0.8) \cup (1.2, 2] \,, \end{array} \right. \tag{9}$$
$$m = 0 \,.$$

Solution profiles for ρ are given for $\varepsilon = 0.8$, $t = 0.5$ and $\varepsilon = 10^{-4}$, $t = 0.05$. These profiles make clear that, while the upwind scheme is satisfactory of $O(1)$ values of ε, it lacks any reasonable sense of accuracy when ε is small. Indeed, the numerical diffusion is so dominant when $\varepsilon = 10^{-4}$, that the profiles for ρ in Figure (1)(a) appear as a flat line. For comparison, a highly resolved reference solution is computed with a second-order, upwind scheme with $20,000$ computational cells.

Higher-order Godunov-type schemes will decrease the numerical dissipation in (7) with respect to h, but the factor of ε^{-1} remains. For example, in smooth regions where a slope-limiter is not needed, the modified system for the second order scheme of Van Leer [42] is [29]

$$\partial_t \rho + \partial_x m = \frac{h^2}{12} \partial_x^3 m - \frac{h^3}{8\sqrt{3}\varepsilon} \partial_x^4 \rho \,, \tag{10a}$$

$$\partial_t m + \frac{1}{3}\frac{1}{\varepsilon^2}\partial_x \rho + \frac{\sigma}{\varepsilon^2} m = \frac{h^2}{36\varepsilon^2} \partial_x^3 m - \frac{h^3}{8\sqrt{3}\varepsilon} \partial_x^4 m \,. \tag{10b}$$

Meanwhile the modified system for the piecewise parabolic method [5], again with no limiter, is [17]

$$\partial_t \rho + \partial_x m = \frac{h^3}{12\sqrt{3}\varepsilon} \partial_x^4 \rho + \frac{h^4}{30} \partial_x^5 m \,, \tag{11a}$$

$$\partial_t m + \frac{1}{3}\frac{1}{\varepsilon^2}\partial_x \rho + \frac{\sigma}{\varepsilon^2} m = \frac{h^3}{12\sqrt{3}\varepsilon} \partial_x^4 m + \frac{h^4}{90\varepsilon^2} \partial_x^5 \rho \,. \tag{11b}$$

In both cases, the numerical dissipation term in the equation for ρ is $O(h^3/\varepsilon)$.

Profiles for ρ computed with a second-order upwind method are displayed in Figures 1(b) and 1(d). When $\varepsilon = 0.8$, the scheme performs well, but when $\varepsilon = 10^{-4}$, the results are strongly dependent on the mesh spacing. For example, with 200 computational cells, $h^3/\varepsilon = 10^{-2}$. Hence the dissipation is relatively small and the solution in 1(d) captures the profile of the reference solution well. However, with 50 computational cells, $h^3/\varepsilon = 0.64$, which means the dissipation term in (10) contributes significantly. As a result the profile is quite smeared.

2.2. **Splitting Method.** The splitting approach introduced in [20, 36] was designed to eliminate the problem of excessive numerical dissipation and to improve the restrictive CFL condition in (8). The idea is to separate the P_1 system into the following components:

(a) $\varepsilon = 0.8$, first order in space and time

(b) $\varepsilon = 0.8$, second order in space and time

(c) $\varepsilon = 10^{-4}$, first order in space and time

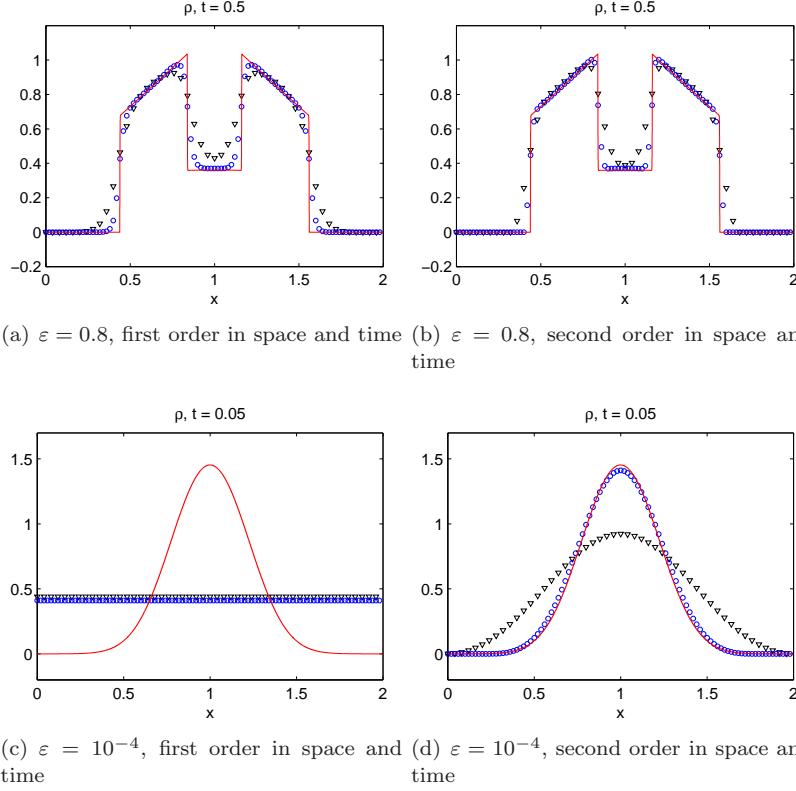(d) $\varepsilon = 10^{-4}$, second order in space and time

FIGURE 1. Standard upwind schemes with periodic boundary conditions and initial condition (9). In all four figures, the triangles represent the solution with $h = .04$, the circles represent the solution with $h = .01$, and the solid line is the highly resolved reference solution that uses $h = 10^{-4}$. The timestep is $\Delta t = 0.1\sqrt{3}\varepsilon h$

.

1. Stiff Component:

$$\partial_t \rho = 0 \,, \tag{12a}$$

$$\partial_t m + \frac{1 - \varepsilon^2}{\varepsilon^2} \frac{1}{3} \partial_x \rho = -\frac{\sigma}{\varepsilon^2} m \,; \tag{12b}$$

2. Non-Stiff Component:

$$\partial_t \rho + \partial_x m = 0 \,, \tag{12c}$$

$$\partial_t m + \frac{1}{3} \partial_x \rho = 0 \,. \tag{12d}$$

For simplicity, we are assuming that $\varepsilon < 1$, although such a restriction is easily lifted [20]. With this splitting, each component is formally well defined. In particular, the non-stiff component is a hyperbolic system with wave speeds $\pm 1/\sqrt{3}$.

The splitting scheme is implemented by updating the stiff component (12a-b) first, using the backward Euler method for the time integration and central differencing to evaluate the spatial derivative of ρ. This gives the intermediate state

$$\rho_j^* = \rho_j^n \,, \tag{13a}$$

$$m^* = \gamma_j m_j^n - \frac{\kappa_j}{3} \frac{\rho_{j+1}^n - \rho_{j-1}^n}{2h} \,, \tag{13b}$$

where

$$\gamma_j := \frac{\varepsilon^2}{\varepsilon^2 + \sigma_j \Delta t} \quad \text{and} \quad \kappa_j := \frac{(1 - \varepsilon^2)\Delta t}{\varepsilon^2 + \sigma_j \Delta t} \,. \tag{14}$$

The non-stiff component is then evaluated with a first order upwind method, using (ρ^*, m^*) for an initial condition:

$$\frac{\rho_j^{n+1} - \rho_j^*}{\Delta t} + \frac{m_{j+1}^* - m_{j-1}^*}{2h} = \frac{1}{\sqrt{3}} \frac{\rho_{j+1}^n - 2\rho_j^n + \rho_{j-1}^n}{2h} \,, \tag{15a}$$

$$\frac{m_j^{n+1} - m_j^*}{\Delta t} + \frac{1}{3} \frac{\rho_{j+1}^n - \rho_{j-1}^n}{2h} = \frac{1}{\sqrt{3}} \frac{m_{j+1}^* - 2m_j^* + m_{j-1}^*}{2h} \,. \tag{15b}$$

Because ρ does not evolve in the stiff step (13), the implementation of the two steps is essentially explicit.

Alternating evaluation of the two steps in (13) and (15) produces a first order scheme. Second-order accuracy in space can be easily obtained using a MUSCL approach to update the non-stiff component. However, second order temporal accuracy requires a more advanced time integrator such as the one used in [20] or one of the IMEX methods discussed in [37, 38].

It is straightforward to show that the splitting method produces an AP scheme. Indeed, as $\varepsilon \to 0$, (13b) becomes a consistent discretization of the balance in (3a):

$$m^* = \frac{1}{3\sigma_j} \frac{\rho_{j+1}^n - \rho_{j-1}^n}{2h} \,. \tag{16}$$

When substituted into (15a), the relation in (16) yields a consistent discretization of the diffusive flux in (3b). Moreover, unlike the semidiscrete upwind discretization (7), the numerical dissipation term in (15a) is independent of ε.

The splitting scheme also has a less restrictive CFL condition than the upwind scheme. In particular, one need only satisfy the two CFL conditions

$$\frac{\gamma \Delta t}{\varepsilon} < Ch \quad \text{and} \quad \kappa \Delta t < C\frac{h^2}{2}, \tag{17}$$

for some $O(1)$ constant C. These two conditions correspond the hyperbolic and diffusive behavior of the P_1 system, respectively. When $\varepsilon < C\sigma h$, the hyperbolic condition on the left will be satisfied independently of the choice of Δt and, as $\varepsilon \to 0$, the condition on the right becomes the standard time step condition for an explicit diffusion equation:

$$\Delta t < \frac{C\sigma h^2}{2} \,. \tag{18}$$

Using the splitting approach, we repeat the same set of numerical experiments that were performed with the upwind schemes: with $\sigma = 1.0$, periodic boundary conditions, and initial conditions given by (9). Results are presented in Figure 2. When $\varepsilon = 0.8$, the splitting method and upwind method give very similar results at both first and second order. When $\varepsilon = 10^{-4}$, the splitting method is more accurate than the upwind method, particularly at first order and with the coarser mesh.

Unfortunately, the profile for the splitting method on the coarse mesh contains what appears to be binary oscillations.

Oscillations, such as those in bottom two plots of Figure 2, are an obvious drawback of the splitting method. In addition to these binary oscillations, other types of oscillations appear in other problems. In Figure 3(a), for example, oscillations appear in the ρ profile of an experiment that uses the discontinuous cross-section

$$\sigma = \begin{cases} 0.02, & x \in [0.35, 0.65] \cup [1.35, 1.65], \\ 1.0, & x \in [0, 0.35) \cup (0.65, 1.35) \cup (1.65, 2]. \end{cases} \tag{19}$$

This profile is computed using a first order splitting scheme with $\varepsilon = 0.1$ and the same initial condition (9). Clearly, non-physical oscillations occur in the regions where σ is smaller. These oscillations appear dispersive and are not restricted to discontinuous cross-sections. For example, similar oscillations also occur when the cross-section is set to the constant value $\sigma = 0.02$, as is depicted Figure 3(b). These results are of particular concern because the oscillations cause the profile to go negative. The highly resolved "true" solution in these figures is generated with a second-order in space and time upwind scheme with $h = .01$. This spatial step resolves the mean free path, and the numerical diffusion is $O(h^3/\varepsilon) = O(10^{-5})$.

3. **A Closer Look at Operator Splitting.** In this section, we take a closer look at the operator splitting method, in an attempt to diagnose and correct oscillations discussed at the end of the previous section. For simplicity, we focus on the first order implementation, in which case updating the state of the P_1 system from (ρ^n, m^n) to (ρ^{n+1}, m^{n+1}) requires one iteration of the two steps in (13) and (15). The complete scheme is

$$\frac{\rho_j^{n+1} - \rho_j^n}{\Delta t} + \frac{\gamma_{j+1} m_{j+1}^n - \gamma_{j-1} m_{j-1}^n}{2h} = \frac{1}{3} \frac{\kappa_{j+1}(\rho_{j+2}^n - \rho_j^n) - \kappa_{j-1}(\rho_j^n - \rho_{j-2}^n)}{4h^2}$$

$$+ \frac{1}{\sqrt{3}} \frac{\rho_{j+1}^n - 2\rho_j^n + \rho_{j-1}^n}{2h} , \tag{20a}$$

$$\frac{m_j^{n+1} - m_j^n}{\Delta t} + \frac{\beta_j}{3\varepsilon^2} \frac{\rho_{j+1}^n - \rho_{j-1}^n}{2h} + \frac{\gamma_j \sigma_j}{\varepsilon^2} m_j^n = \frac{1}{\sqrt{3}} \frac{\gamma_{j+1} m_{j+1}^n - 2\gamma_j m_j^n + \gamma_{j-1} m_{j-1}^n}{2h}$$

$$- \frac{1}{3\sqrt{3}} \frac{\kappa_{j+1}(\rho_{j+2}^n - \rho_j^n) - 2\kappa_j(\rho_{j+1}^n - \rho_{j-1}^n) + \kappa_{j-1}(\rho_j^n - \rho_{j-2}^n)}{4h^2} , \tag{20b}$$

where γ_j and κ_j are given in (14) and

$$\beta_j := \gamma_j + \varepsilon^2(1 - \gamma_j) . \tag{21}$$

Two terms in (20) immediately stand out as a possible source of oscillations. First is the numerical diffusion term in (20a):

$$\frac{\kappa_{j+1}(\rho_{j+2}^n - \rho_j^n) - \kappa_{j-1}(\rho_j^n - \rho_{j-2}^n)}{4h^2} = \partial_x(\kappa \partial_x \rho) + O(h) , \tag{22}$$

which is based on a wide stencil that uses every other cell—a so-called *black-red discretization*. In [15], it is speculated that this stencil makes the scheme susceptible to binary oscillations. The other obvious candidate is the numerical dispersion term

(a) $\varepsilon = 0.8$, first order in space and time

(b) $\varepsilon = 0.8$, second order in space and time

(c) $\varepsilon = 10^{-4}$, first order in space and time

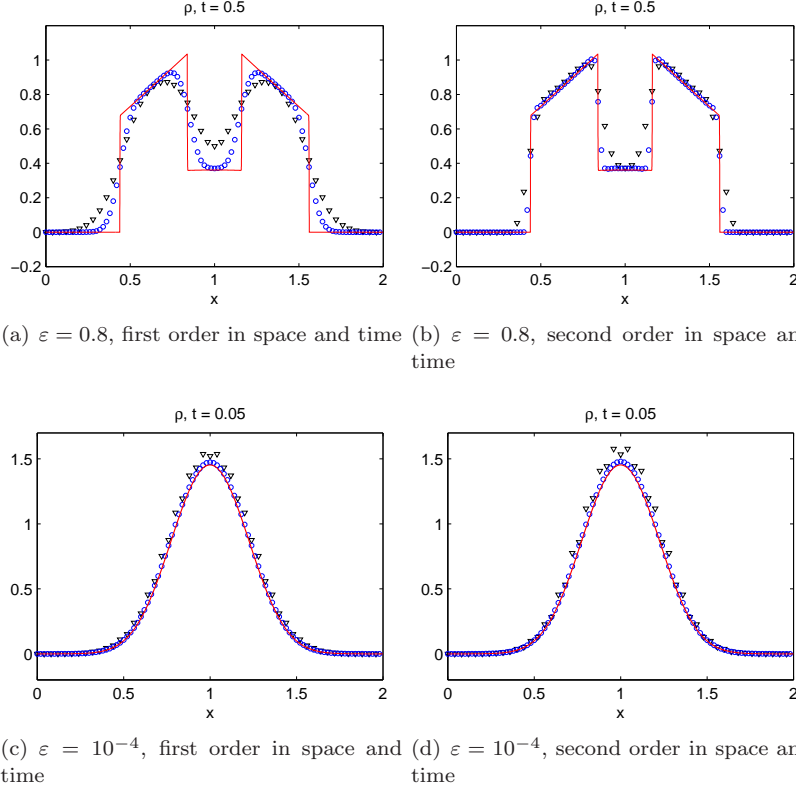(d) $\varepsilon = 10^{-4}$, second order in space and time

FIGURE 2. The splitting scheme, with periodic boundary conditions and initial condition (9). In all four figures, the triangles represent the solution with $h = 0.04$, the circles represent the solution with $h = 0.01$, and the solid line is a highly resolved "true" solution with $h = 10^{-4}$. The timesteps are chosen using the CFL condition (17) with $C = 0.1$

in (20b):

$$\frac{\kappa_{j+1}(\rho_{j+2}^n - \rho_j^n) - 2\kappa_j(\rho_{j+1}^n - \rho_{j-1}^n) + \kappa_{j-1}(\rho_j^n - \rho_{j-2}^n)}{4h^2} = \frac{h}{2}\partial_x(\kappa\partial_x^2\rho) + O(h^2).$$
(23)

The presence of this term and the subtle numerical issues it poses has been noted in [16].

We first address the oscillations in Figures 2 (c) and (d). Because the oscillations appear to be binary, we replace the staggered diffusion discretization in (20) with a more standard discretization:

$$\frac{\kappa_{j+1}(\rho_{j+2}^n - \rho_j^n) - \kappa_{j-1}(\rho_j^n - \rho_{j-2}^n)}{4h^2} \rightarrow \frac{\kappa_{j+1/2}(\rho_{j+1}^n - \rho_j^n) - \kappa_{j-1/2}(\rho_j^n - \rho_{j-1}^n)}{h^2}.$$
(24)

where $\kappa_{j+1/2}$ is the harmonic average of κ_j and κ_{j+1}. It is clear from Figure 4(a) that this change has fixed the problem.

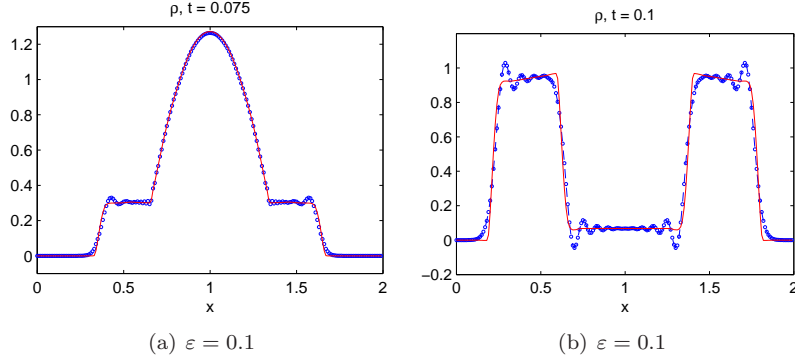(a) $\varepsilon = 0.1$ (b) $\varepsilon = 0.1$

FIGURE 3. Left: The splitting scheme with the discontinuous cross-section given by (19) and initial condition given by (9), $\varepsilon = 0.1$, and $t = 0.075$. Right: The first order in space and time splitting scheme with a constant cross-section of $\sigma = 0.02$, initial condition given by (9), $\varepsilon = 0.1$, and $t = 0.1$. In both figures, the circles represent numerical solution with a first order accurate scheme with $h = 0.01$ and the solid line is a "true" solution computed with a second-order in space and time upwind scheme with $h = .01$. The timesteps are chosen using the CFL condition (17) with $C = 0.1$

It should also be noted that for the *smooth* initial condition

$$\rho = e^{-10(x-1)^2} \quad \text{and} \quad m = 0 \,, \tag{25}$$

there are no oscillations. See Figure 4(b). Thus we conclude that these binary oscillations are associated with the discontinuity in the initial condition (9).
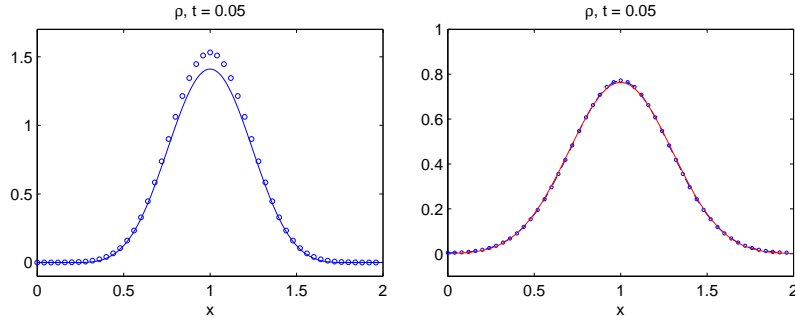

FIGURE 4. On the left, a recalculation of Figure 2 (c), with the black-red diffusion discretization replaced with a standard discretization, as described in (24). On the right, the black-red discretization is kept, but the smooth initial condition (25) is used.

The next task is to determine the cause of oscillations depicted in Figure 3. These oscillations appear dispersive, so our first inclination is to remove the dispersive

term (23) from (20). Because this term is $O(h)$, removing it does not affect the consistency of the scheme. Unfortunately, it is clear from Figure 5(a) that the oscillatory behavior does not improve. We also try replacing the black-red diffusion discretization with the standard discretization in (24). However, as Figure 5(b) shows, the oscillations remain.
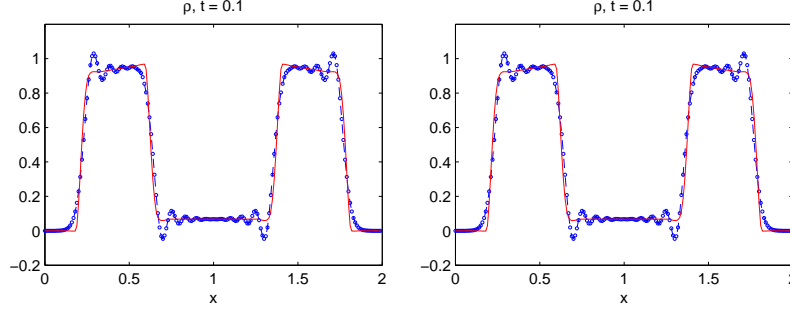

FIGURE 5. Left: Splitting scheme with dispersive term removed. Right: Splitting scheme with staggered diffusion term modified.

It turns out that one way to suppress the oscillations in Figure 3 can be determined by the modified equations for (20), which have the form

$$\partial_t \rho + \partial_x(\gamma m) = \frac{1}{3}\partial_x(\kappa\partial_x\rho) + \frac{h}{2\sqrt{3}}\partial_x^2\rho \,, \tag{26a}$$

$$\partial_t m + \frac{1}{3}\beta\partial_x\rho + \frac{\gamma\sigma}{\varepsilon^2}m = \frac{h}{2\sqrt{3}}\partial_x^2(\gamma m) - \frac{h}{6\sqrt{3}}\partial_x(\kappa\partial_x^2\rho) \,, \tag{26b}$$

where κ, β, γ are now functions of x. These modified equations are an $O(h, \Delta t)$ approximation of the following hyperbolic parabolic system:

$$\partial_t \rho + \partial_x(\gamma m) = \frac{1}{3}\partial_x(\kappa\partial_x\rho) \,, \tag{27a}$$

$$\partial_t m + \frac{1}{3}\frac{\beta}{\varepsilon^2}\partial_x\rho = -\frac{\gamma\sigma}{\varepsilon^2}m \,, \tag{27b}$$

which, to our knowledge, was first derived for a constant cross-section in [16]. Following the work in [16], a similar set of modified equations was derived in [15] for general P_N systems [26, 39] in one dimension, but with spatially varying cross-sections.

For a constant cross-section, a first-order semi-discrete method for (27) is given by

$$\partial_t \rho_j + \gamma\frac{m_{j+1} - m_{j-1}}{2h} = \frac{h}{2\varepsilon}\sqrt{\frac{\beta\gamma}{3}}\frac{\rho_{j+1} - 2\rho_j + \rho_{j-1}}{h^2} \,, \tag{28a}$$

$$\partial_t m_j + \frac{1}{\varepsilon^2}\frac{\beta}{3}\frac{\rho_{j+1} - \rho_{j-1}}{2h} + \frac{\sigma_j}{\varepsilon^2}m_j = \frac{h}{2\varepsilon}\sqrt{\frac{\beta\gamma}{3}}\frac{m_{j+1} - 2m_j + m_{j-1}}{h^2} \,. \tag{28b}$$

The numerical dissipation terms, which are necessary for stability and suppression of oscillations, are on the right. Meanwhile, the discretization for (27) given by the splitting has numerical dissipation terms of the form of

$$\frac{1}{\sqrt{3}}\frac{\rho_{j+1}^n - 2\rho_j^n + \rho_{j-1}^n}{2h} \quad \text{and} \quad \frac{\gamma}{\sqrt{3}}\frac{m_{j+1}^n - 2m_j^n + m_{j-1}^n}{2h} \,. \tag{29}$$

We conclude that the splitting scheme in (20) suffers from *too little* numerical dissipation, as opposed to a standard upwind solver, which uses too much . If we replace the dissipation terms in (20) by the corresponding dissipation terms in (27), the oscillations in Figure 3 disappear and we obtain the correct behavior. These results are presented in Figure 6 (a) and (b) for both the constant and non-constant cross-section.

Rather than repeat our analysis for the second order version of the splitting scheme (a much more tedious task), we work directly with the modified system (27). For a non-constant cross-section, discretization of this system is a challenge because it is not in conservative form. Here the splitting scheme provides some guidance. In particular, the form of the dissipation terms in (20) suggests the appropriate discretization for (27). In terms of the variables ρ and $q := \beta^{-1}m$, the modified system (27) takes the form

$$\partial_t \rho + \partial_x(\gamma\beta q) = \frac{1}{3}\partial_x(\kappa\partial_x\rho) \, , \tag{30a}$$

$$\partial_t q + \frac{1}{3\varepsilon^2}\partial_x\rho = -\frac{\gamma\sigma}{\varepsilon^2}q \, . \tag{30b}$$

This system is now in conservative form, but with spatially varying fluxes. It therefore requires a generalization of the upwind treatment. Details of the scheme are given in the appendix. Results that are first-order and time, but second-order in space are presented in figures 6 (b) and (d). The profiles in these figures are very accurate, even though the time integration is only first-order.

4. **Discussion and Conclusions.** We have presented a computational study of an operator splitting method for the P_1 equations. Our results show that small modifications are sometimes needed to suppress numerical oscillations in the method. In some cases, we have found that discretization of diffusion terms on a black-red stencil can introduce binary oscillations into the numerical solution. In other cases there is simply not enough numerical dissipation to suppress oscillations.

The examples presented here are not exhaustive. Indeed, a more complete analysis of the splitting scheme would be needed to conclude that the scheme is completely free of oscillations. For example, one could attempt to establish some notion of a total variation diminishing (TVD) property or, more generally, a positivity property in the sense of Lax and Liu [28].

While oscillations of an isolated system may be stable, they may introduce instabilities when coupled to large multi-physics codes. For example, it is important to ensure that a numerical scheme does not produce false minima or maxima. Moving forward, it seems that a more robust approach is to use modified systems like (27). This approach has seen some initial success [16, 15], but the presence of non-conservative products in these systems presents a major obstacle. In this respect, operator splitting schemes may continue to provide insight into how to appropriately discretize modified systems.

(a) first order in space

(b) first order in space
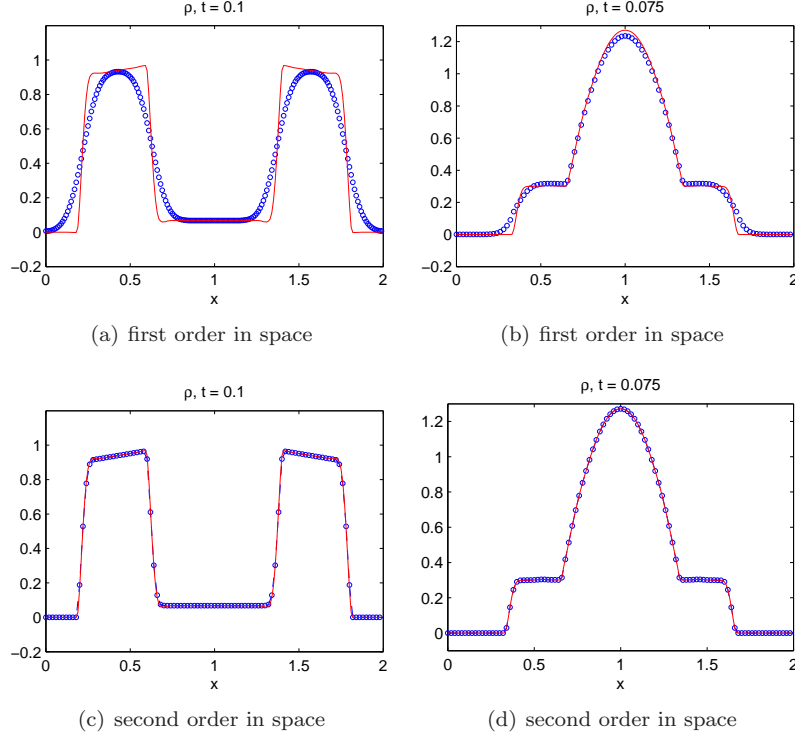
(c) second order in space

(d) second order in space

FIGURE 6. Left: P_1 solution at time $t = 0.1$ with constant cross-section $\sigma = 0.02$. Right: Solution at time $t = 0.075$ with the discontinuous cross section given by (19). In both figures, the solid line is the reference solution and the circles are the solution using the splitting method with the corrected numerical diffusion. The timestep is chosen using the CFL conditions (17) with $C = 0.1$

5. **Appendix.** The purpose of this appendix is to provide complete details of the schemes used to produce the results presented in the paper. As in the main text, all state variables and the cross-section σ are adorned with the subscript j to denote an average value over a computational cell I_j with width h. The parameters γ_j, β_j, and κ_j are composite parameters that depend on σ via the relations given in (14) and (21). Supscripts of the form $j \pm 1/2$ denote pointwise values, or approximations thereof, at cell edges.

5.1. **A Few Basic Tools.** Many of the schemes in the paper use the following tools.

Discretization of Linear Flux Gradients. Let $A\mathbf{u}_x$ be a linear flux in a hyperbolic system, with A a constant matrix. A finite volume discretization of $A\mathbf{u}_x$ is given by

$$\int_{x_{j-1/2}}^{x_{j+1/2}} A\mathbf{u}_x \, dx = A(\mathbf{u}_{j+1/2} - \mathbf{u}_{j-1/2})$$

$$\simeq \frac{1}{2}A\left(\mathbf{u}_{j+1/2,\ell} + \mathbf{u}_{j+1/2,r}\right) + \frac{1}{2}|A|\left(\mathbf{u}_{j+1/2,\ell} - \mathbf{u}_{j+1/2,r}\right) . \quad (31)$$

Here the t-dependence of $\mathbf{u}$ has been suppressed and the matrix $|A| := R|\Lambda|R^{-1}$ is calculated using the eigenvectors and eigenvalues in the diagonalization decomposition $A = R\Lambda R^{-1}$. The right and left edge values of $\mathbf{u}$ in (31) are given by

$$\mathbf{u}_{j+1/2,\ell} = R\mathbf{w}_{j+1/2,\ell} \quad \text{and} \quad \mathbf{u}_{j+1/2,r} = R\mathbf{w}_{j+1/2,r}\,, \tag{32}$$

and the characteristic edge values are determined by linear reconstructions on adjacent cells; that is,

$$\mathbf{w}_{j+1/2,\ell} = \mathbf{w}_j + \frac{h}{2}\mathbf{w}'_j \quad \text{and} \quad \mathbf{w}_{j+1/2,r} = \mathbf{w}_{j+1} - \frac{h}{2}\mathbf{w}'_{j+1}\,, \tag{33}$$

where $\mathbf{w}_j := R^{-1}\mathbf{u}_j$ and the slopes $\mathbf{w}'_j$ approximate derivatives in each cell. We use three different approximations for the slope: (i) zero slope; (ii) central difference; and (iii) the double minmod limiter:

$$\mathbf{w}'_j = \frac{1}{h}\,\text{minmod}\left(2(\mathbf{w}_{j+1} - \mathbf{w}_j), \frac{1}{2}(\mathbf{w}_{j+1} - \mathbf{w}_{j-1}), 2(\mathbf{w}_j - \mathbf{w}_{j-1})\right)\,, \tag{34}$$

which is applied to vectors component-wise.

Second-Order Time Integration. For second-order time integration, we use two methods: a TVD Runge-Kutta method and an IMEX method. For an ODE of the form

$$\dot{y} = L(y)\,, \tag{35}$$

with L linear, a second-order Runge Kutta scheme is [12, 40]

$$\mathbf{y}^{(1)} = \mathbf{y}^n + \Delta t L(\mathbf{y}^n)\,, \tag{36a}$$

$$\mathbf{y}^{n+1} = 0.5[\mathbf{y}^n + \mathbf{y}^{(1)} + \Delta t L(\mathbf{y}^{(1)})]\,. \tag{36b}$$

Given $L = L_1 + L_2$, the following IMEX scheme [38, 37] is used when an explicit update of L_1 and an implicit update of L_2 is desired.

$$\mathbf{y}^{(1)} = \mathbf{y}^n + \Delta t\eta L_2(\mathbf{y}^{(1)})\,, \tag{37a}$$

$$\mathbf{y}^{(2)} = \mathbf{y}^n + \Delta t[L_1(\mathbf{y}^{(1)}) + (1 - 2\eta)L_2(\mathbf{y}^{(1)}) + \eta L_2(\mathbf{y}^{(2)})]\,, \tag{37b}$$

$$\mathbf{y}^{n+1} = \mathbf{y}^n + \frac{\Delta t}{2}[L_1(\mathbf{y}^{(1)}) + L_1(\mathbf{y}^{(2)}) + L_2(\mathbf{y}^{(1)}) + L_2(\mathbf{y}^{(2)})]\,. \tag{37c}$$

where

$$\eta = 1 - \frac{1}{\sqrt{2}}. \tag{38}$$

5.2. **The Schemes.** We now present the details for the upwind and splitting schemes used to produce results in the main paper. We also write out the details for discretizing the regularized system (30).

Upwind scheme. Let $\mathbf{u} = (\rho, m)^T$. Then the upwind discretization of (1) is given by

$$d_t\mathbf{u}_j + A_\varepsilon\frac{(\mathbf{u}_{j+1/2} - \mathbf{u}_{j-1/2})}{h} = -\sigma_j Q_\varepsilon\mathbf{u}_j\,, \tag{39}$$

where

$$A_\varepsilon = \begin{pmatrix} 1 & 0 \\ 0 & \frac{1}{3\varepsilon^2} \end{pmatrix} \quad \text{and} \quad Q_\varepsilon = \begin{pmatrix} 0 & 0 \\ 0 & \frac{1}{\varepsilon^2} \end{pmatrix}\,. \tag{40}$$

Note that the time dependence of $\mathbf{u}$ has been suppressed. The evaluation of the fluxes $A_\varepsilon\mathbf{u}_{j\pm1/2}$ is given by (31) with $A = A_\varepsilon$. For the test cases in Figure 1, a first order spatial discretization is accomplished by setting the slope in (33) to zero. This is exactly (5). Meanwhile, the second order version uses the double minmod

limiter (34). The time integration of (39) is accomplished with a first-order forward Euler scheme, and with the second-order IMEX scheme in (37), treating the flux terms explicitly and the source term implicitly.

The highly resolved reference solutions, which are used for comparison in all the figures, are computed with an upwind method. However, its exact implementation depends on the value ε. For $\varepsilon = 0.8$, the spatial reconstruction uses the double minmod limiter (34) and the Runge-Kutta method (36a). Thus the scheme is fully second order. For $\varepsilon = 10^{-4}$ the solution is presumably smooth, so the spatial derivative in (33) is computed using a central difference—with no limiting— in order to obtain second-order spatial accuracy. However, only a first order time integrator is used, with the source term treated implicitly and the flux term explicitly. Because (8) is so restrictive, $\Delta t \sim h^2$, and a second-order time integrator is not really needed.

Splitting Scheme. For the splitting scheme, the implicit step (12a) is accomplished by using (13) for both first and second-order as

$$d_t \mathbf{u}_j + A_1 \frac{(\mathbf{u}_{j+1/2} - \mathbf{u}_{j-1/2})}{dx} = 0\,, \tag{41}$$

where $\mathbf{u}_j = (\rho_j^*, m_j^*)$ (see (13)) and

$$A_1 = A_{\varepsilon=1} = \begin{pmatrix} 1 & 0 \\ 0 & \frac{1}{3} \end{pmatrix}\,. \tag{42}$$

As in the upwind discretization above, the evaluation of the fluxes $A\mathbf{u}_{j\pm1/2}$ is determined by (31), except this time with $A = A_1$. At first order, the slope approximation in (33) is set to zero; at second order the double minmod limiter (34) is used. Time integration at first order involves alternating evaluation of the two steps in (13) and (15). To get second order in time, the IMEX scheme (37) is used, where L_1 represents the non-stiff step and L_2 represents the stiff step.

The first order version of the splitting scheme is given explicitly in (20), and first-order modifications to this scheme, which were to suppress the non-physical oscillations, are described explicitly in Section 3. Rather than directly implement similar modifications to the second-order splitting method, we instead work with the regularized system (30).

Regularized Equations. The numerical scheme for regularized system (30) (which was used to generate the profile in Figures 6(c) and 6(d)) can be formulated as a generalization of the upwind method for spatially varying fluxes. However, it is simpler to write out the scheme in terms of the components ρ and q. In semi-discrete form, the scheme is

$$\partial_t \rho_j + \frac{(\gamma\beta q)_{j+1/2} - (\gamma\beta q)_{j-1/2}}{h} = \frac{1}{3} \frac{\kappa_{j+1/2}(\rho_{j+1}^n - \rho_j^n) - \kappa_{j-1/2}(\rho_j^n - \rho_{j-1}^n)}{h^2}\,, \tag{43a}$$

$$\partial_t q_j + \frac{1}{3\varepsilon^2} \frac{\rho_{j+1/2} - \rho_{j-1/2}}{h} = -\frac{\gamma_j \sigma_j}{\varepsilon^2} q_j\,. \tag{43b}$$

where $\kappa_{j+1/2}$ is the harmonic average of surrounding cell values:

$$\kappa_{j+1/2} = \frac{2\kappa_j \kappa_{j+1}}{\kappa_j + \kappa_{j+1}}\,. \tag{44}$$

To compute edge values in (43), we define the diagonal variables

$$w^\pm = \rho + \sqrt{3\gamma\beta}\varepsilon q\,, \tag{45}$$

so that

$$\rho_{j+1/2} = \frac{1}{2}(w^+_{j+1/2} + w^-_{j+1/2}) \quad \text{and} \quad (\gamma\beta q)_{j+1/2} = \frac{1}{2\varepsilon}\sqrt{\frac{(\gamma\beta)_{j+1/2}}{3}}(w^+_{j+1/2} - w^-_{j+1/2}). \tag{46}$$

Because of the spatial variation in γ and β, two upwinding steps are needed. First the edge values $w^{\pm}_{j+1/2}$ are determined in standard fashion:

$$w^+_{j+1/2} = w^+_{j+1/2,l} \quad \text{and} \quad w^-_{j+1/2} = w^-_{j+1/2,r}, \tag{47}$$

where the left and right values are based on linear reconstructions:

$$w^+_{j+1/2,l} = w^+_j + \frac{h}{2}s^+_j \quad \text{and} \quad w^-_{j+1/2,r} = w^+_{j+1} - \frac{h}{2}s^-_j, \tag{48}$$

and the slopes $s^{\pm}$ are approximated with the double minmod limiter (34). Next, the products $(\sqrt{\gamma\beta}w^{\pm})_{j+1/2}$ in (46) are computed as

$$\left(\sqrt{\gamma\beta}w^+\right)_{j+1/2} = \sqrt{(\gamma\beta)_{j+1/2,\ell}}\,w^+_{j+1/2,\ell} \tag{49}$$

$$\left(\sqrt{\gamma\beta}w^-\right)_{j+1/2} = \sqrt{(\gamma\beta)_{j+1/2,r}}\,w^+_{j+1/2,r} \tag{50}$$

where $(\gamma\beta)_{j+1/2,r}$ and $(\gamma\beta)_{j+1/2,\ell}$ are calculated with the same type of linear reconstruction as in (48), again with the double minmod limiter.

For constant cross-section, the approach described here reduces to a standard second order upwind method. We use this method with a forward Euler time integrator for (43) to compute solutions in Figures 6 (c) and (d). Thus the scheme is second order in space, but only first order in time.

REFERENCES

[1] U. M. ASCHER AND L. R. PETZHOLD, "Computer Methods for Ordinary Differential Equations and Differential-Algebraic Equations", SIAM, Philadelphia, 1999.

[2] C. BUET AND S. CORDIER, *Asymptotic preserving scheme and numerical methods for radiative hydrodynamic models*, C. R. Acad. Sci Paris, Ser. I, **338** (2004), pp. 951–956.

[3] C. CATTANEO, *On the conduction of heat*, Atti Del Seminar. Mat. Fis. Univ., Modena, **3** (1948), pp. 3–21.

[4] C. CATTANEO, *Sur une forme de lequation de la chaleur eliminant le paradoxe dune propagation instantanee*, Comptes Rendus Acad. Sci., **247** (1958), pp. 431 – 433.

[5] P. COLLELA AND P. R. WOODWARD, *The piecewise parabolic method (ppm) for gas-dynamical simulations*, J. Comput. Phys., **54** (1984), pp. 174–201.

[6] F. FILBET AND B. P. PH. LAURENÇOT, *Derivation of hyperbolic models for chemosensitive movement*, J. Math. Biol., **50** (2005), pp. 189–2007.

[7] F. FILBET AND C.-W. SHU, *Approximation of hyperbolic models for chemosensitive movement*, SIAM J. Sci. Comp., **27** (2005), pp. 850–872.

[8] G. NALDI AND L. PARESCHI, *Numerical schemes for hyperbolic systems of conservation laws with stiff diffusive relaxation*, Applied Math. Letters, **11** (1998), pp. 29–35.

[9] S. GOLDSTEIN, *On diffusion by discontinuous movements, and on the telegraph equation*, Quart. J. Mech. Appl. Math., **4** (1951), pp. 129–156.

[10] L. GOSSE AND G. TOSCANI, *An asymptotic-preserving, well-balanced scheme for the hyperbolic heat equations*, C. R. Acad. Sci. Paris, Ser. I, **334** (2002), pp. 337–342.

[11] L. GOSSE AND G. TOSCANI, *Asymptotic-preserving and well-balance schemes for radiative transfer and the Rosseland approximation*, Numerische Mathematik, **98** (2004), pp. 223–250.

[12] S. GOTTLIEB AND C.-W. SHU, *Total variation diminishing runge-kutta schemes*, Mathematics of Computation, **67** (1998), pp. 73–8.

[13] M. GURTIN AND A. C. PIPKIN, *A general theory of heat conduction, with finite wave speeds*, Arch. Rational Mech. Anal., **31** (1968), pp. 113–126.

[14] C. D. HAUCK, "Entropy-Based Moment Closures in Semiconductor Models", Ph.D thesis, University of Maryland, College Park, 2006.

[15] C. D. HAUCK AND R. B. LOWRIE, *Temporal regularization of the P_N equations*, Los Alamos Report LA-UR 07-7995, to appear in SIAM J. Multiscale Modeling and Analysis, (2008).

[16] S. JIN, *Efficient asymptotic preserving (AP) schemes for some multiscale kinetic equations*, SIAM J. Sci. Comp., **21** (1999), pp. 441–454.

[17] S. JIN AND C. D. LEVERMORE, *Discretization of the multiscale semiconductor Boltzmann equation by diffusive relaxation schemes*, J. Comp. Phys., **126** (2000), pp. 312–330.

[18] S.JIN AND L.PARESCHI, *Discretization of the multiscale semiconductor boltzmann equation by diffusive relaxation schemes*, J. Comp. Phys., **161** (2000), pp. 312–330.

[19] S. JIN AND L. PARESCHI, *Asymptotic-Preserving (AP) Schemes for Multiscale Kinetic Equations: a Unified Approach*, in "Hyperbolic Problems: Theory, Numerics, Applications" (eds. H. Freistühler and G. Warneke), Birkhauser-Verlag, Berlin, (2001), pp. 573–582.

[20] S. JIN, L. PARESCHI, AND G. TOSCANI, *Diffusive relaxation schemes for multiscale discrete-velocity kinetic equations*, SIAM J. Numer. Anal., **35** (1998), pp. 2405–2439.

[21] S. JIN, L. PARESCHI, AND G. TOSCANI, *Uniformly accurate diffusive relaxation schemes for multiscale transport equations*, SIAM J. Numerical Analysis, **98** (2000), pp. 913–936.

[22] T. G. KURTZ, *Convergence of sequences of semigroups of nonlinear operators with an application to gas kinetics*, Trans. Amer. Math. Soc., **186** (1973), pp. 259–272.

[23] E. W. LARSEN AND J. D'ARRUDA, *Asymptotic theory of the linear transport equations for small mean free paths, i*, Phys. Rev. A, **13** (1976), pp. 1933–1939.

[24] E. W. LARSEN AND J. E. MOREL, *Asymptotic solutions of numerical transport problems in optically thick, diffusive regimes. ii.*, Journal of Computational Physics, **83** (1989), pp. 212–36.

[25] C. D. LEVERMORE, *Relating Eddington factors to flux limiters*, J. Quant. Spectrosc. Radiat. Transfer, **31** (1984), pp. 149–160.

[26] E. E. LEWIS AND J. W. F. MILLER, "Computational Methods in Neutron Transport", John Wiley and Sons, New York, 1984.

[27] P.-L. LIONS AND G. TOSCANI, *Diffusive limit for finite velocity Boltzmann kinetic models*, Rev. Mat Iberoamericana, **13** (1997), pp. 473–513.

[28] X.-D. LIU AND P. LAX, *Positive schemes for solving multi-dimensional hyperbolic systems of conservation laws*, J. Comput. Phys., **5** (1996), p. 133156.

[29] R. B. LOWRIE AND J. E. MOREL, *Methods for hyperbolic systems with stiff relaxation*, Int. J. Numer. Meth. Fluids, **40** (2002), pp. 413–423.

[30] P. MARCATI AND B. RUBINO, *Parabolic relaxation limit for hyperbolic systems of conservation laws*, Proceedings of the VIII conference on Waves and Stability, (1996), pp. 393–406.

[31] P. MARCATI AND B. RUBINO, *Hyperbolic to parabolic relaxation theory for quasilinear first order systems*, J. Differential Equations, **162** (2000), pp. 359–399.

[32] R. G. MCCLARREN, T. M. EVANS, R. B. LOWRIE, AND J. D. DENSMORE, *Semi-implicit time integration for P_N thermal radiative transfer*, J. Comp. Phys., **227** (2008), pp. 7561–7586.

[33] H. P. MCKEAN, *The central limit theorem for Carlemann's equation*, Israel J. Math, **21** (1975), pp. 54–92.

[34] G. N. MINERBO, *Maximum entropy Eddington factors*, J. Quant. Spectrosc. Radiat. Transfer, **20** (1978), pp. 541–545.

[35] G. B. NAGY, O. E. ORTIZ, AND O. A. REU, *The behavior of hyperbolic heat equations solutions near their parabolic limits*, J. Math. Phys, **35** (1994), pp. 4344 – 4356.

[36] G. NALDI AND L. PARESCHI, *Numerical schemes for hyperbolic systems of conservation laws with stiff diffusive relaxation*, SIAM J. Numer. Anal., **37** (2000), pp. 1246–1270.

[37] L.PARESCHI AND G.RUSSO, *Implicit-Explicit Runge-Kutta schemes for stiff systems of differential equations*, Nova Science Publishers, **3**, (2000), pp. 269–289.

[38] L. PARESCHI AND G.RUSSO, *Implicit-explicit Runge-Kutta methods and applications to hyperbolic systems with relaxation*, J. Sci. Comput., **25** (2005), pp. 129–155.

[39] G. C. POMRANING, "The Equations of Radiation Hydrodynamics", Pergamon Press, New York, 1973.

[40] C.-W. SHU AND S. OSHER, *Efficient implementation of essentially non-oscillatory shock capturing schemes*, J. Comput. Phys., **77** (1988), p. 439471.

[41] G. I. TAYLOR, *Diffusion by continuous movements*, Proc. London Math. Soc., **20** (1921), pp. 196–212.

[42] B. van Leer, *Towards the ultimate conservative diference scheme v. a second-order sequel to Godunovs method*, J. Comput. Phys., **32** (1979), p. 101136.

E-mail address: `haack@math.wisc.edu`

E-mail address: `cdhauck@lanl.gov`